AJNR

Diffusion Tensor Tractography of the Limbic System

Luis Concha, Donald W. Gross and Christian Beaulieu

AJNR Am J Neuroradiol 2005, 26 (9) 2267-2274
http://www.ajnr.org/content/26/9/2267

AJNR Am J Neuroradiol 26:2267–2274, October 2005

Diffusion Tensor Tractography of the Limbic System

Luis Concha, Donald W. Gross, and Christian Beaulieu

BACKGROUND AND PURPOSE: **The limbic system, relevant to memory and emotion, is an interesting subject of study in healthy and diseased individuals. It consists of a network of gray matter structures interconnected by white matter fibers. Although gray matter components of this system have been studied by using MR imaging, the connecting fibers have not been analyzed to the same degree. Cerebrospinal fluid (CSF) signal intensity contamination of the fornix and cingulum, the 2 major white matter tracts of the limbic system, can alter diffusion-tensor imaging (DTI) measurements and affect tractography. We investigated the effect of CSF signal intensity suppression on fiber tracking of the limbic connections and characterized the diffusion properties of these structures in healthy volunteers.**

METHODS: **Nine healthy individuals were scanned with standard and CSF-suppressed DTI. Tractography of the fornix and cingulum was performed for both acquisition methods. We report mean diffusivity and fractional anisotropy measurements of the crus, body, and columns of the fornix, and descending, superior, and anterior portions of the cingulum.**

RESULTS: **Diffusion measurements were improved and tractography was facilitated by using CSF-suppressed DTI. In particular, tract volume increased, whereas decreases of the mean diffusivity and increases of diffusion anisotropy more accurately represented the underlying tissue by minimizing deleterious partial volume averaging from CSF. This was particularly true for the fornix because it is in closest contact to CSF. Diffusion measurements throughout the limbic connections were consistent in healthy volunteers.**

CONCLUSION: **We recommend the use of CSF suppression when performing diffusion-tensor tractography of the limbic system.**

The limbic system plays a very important role in high-level mental processes, such as memory and emotive behavior, and is composed of a group of interconnected gray and white matter structures that create a loop in each cerebral hemisphere (1). In 1937, James Papez (2) described an important set of connections in the limbic system that link the hippocampus, mamillary bodies, thalamus, cingulated, and parahippocampal gyrus. Whereas other structures have subsequently been integrated into the limbic system (such as the amygdala, the septal region, and the olfactory bulb), the circuit of Papez contains most of the principal limbic gray and white matter structures. The 2 most visible white matter connections in this circuit are the fimbria/fornix, which projects from the hippocampus to the septal region and mamillary bodies, and the cingulum, which connects the enthorinal cortex and the cingulate gyrus.

Both the gray and white matter components of the limbic system have been studied by using MR imaging in several brain disorders, such as epilepsy (3–7), dementia (8, 9), and schizophrenia (10). Until recently, the study of white matter bundles was restricted to postmortem dissection or section-by-section evaluation by in vivo medical imaging both in terms of the tissue's signal intensity and/or volume measurements. Recent advancements in MR imaging, however, allow virtual in vivo dissection of major white matter bundles in the brain (11). White matter fibers are depicted on the basis of the behavior of water movement, as measured with diffusion-tensor imaging (DTI), and are later reconstructed in 3 dimensions by using a technique known as diffusion-tensor tractography (12–15).

DTI can provide indirect measures of the func-

Received December 12, 2004; accepted after revision April 23, 2005.

From the Department of Biomedical Engineering (L.C., C.B.) and the Division of Neurology, Department of Medicine (D.W.G.), University of Alberta, Edmonton, Alberta, Canada.

Operating and salary support was provided by the Alberta Heritage Foundation for Medical Research and Canadian Institutes of Health Research (to C.B.), Promep (to L.C.), and the Savoy Foundation (to D.W.G.).

Presented at the 12th scientific meeting and exhibition of the International Society of Magnetic Resonance in Medicine, May 15–21, 2004, Kyoto, Japan.

Address correspondence to Christian Beaulieu, PhD, Department of Biomedical Engineering, 1098 Research Transition Facility, University of Alberta, Edmonton, AB T6G 2V2, Canada.

tional integrity of white matter and has been previously used in the study of limbic structures both in healthy (16) and diseased individuals (17–21). Diffusion measurements are usually performed by manually defining regions of interest on 2D image maps or by performing voxel-based analysis of spatially normalized images. Manual drawing of regions of interest has 3 disadvantages: (1) it is user dependent, (2) it is time consuming (regions of interest must be drawn section by section); and (3) it is sometimes very difficult to delineate a white matter bundle solely on the basis of anatomic scans and/or diffusion anisotropy maps. Although voxel-based analysis (eg, statistical parametric mapping [SPM]) does not suffer any of these disadvantages, image datasets must be normalized to a standard space by means of nonlinear registration, the downside being that the original data are typically modified and smoothed with a Gaussian filter—to satisfy statistical assumptions and compensate for the imperfections of the spatial normalization (22, 23).

The use of tractography to outline a volume from which to extract various diffusion parameters (ie, mean diffusivity, fractional anisotropy [FA]) is a promising technique (24–26) because it diminishes the 3 disadvantages of manual region of interest drawing and does not require spatial normalization of the images. White matter bundles are segmented semiautomatically by means of tractography by using tract selection regions that are less susceptible to user bias than region of interest drawing. Such an approach has been shown to be reproducible (25) and is typically faster than manual region of interest–based analyses. The poor delineation of the cingulum and fornix on apparent diffusion coefficient (ADC) or FA 2D maps, coupled with their curved trajectories, make tractography an ideal tool for their study. Diffusion-tensor tractography has been used to delineate the fornix and/or cingulum in healthy volunteers (11, 16, 27), as well as patients with epilepsy (21), but, to the best of our knowledge, no study has reported the diffusion characteristics of all the different portions of the fornix (crus, body, and columns) and cingulum (descending, superior, and anterior portions) in healthy, young adults.

Because the fornix and cingulum are adjacent to CSF spaces (ie, the ventricles and interhemispheric fissure), the delineation of the tracts and their absolute diffusion parameters may be adversely affected by partial volume with the rapid, isotropically diffusing CSF. The use of a fluid-attenuated inversion recovery (FLAIR) (28) component before a DTI imaging sequence greatly minimizes CSF signal intensity contamination, though at the expense of a significant increase in acquisition time and a reduction in signal intensity–to-noise ratio (SNR; 29–31). The effects of CSF signal intensity suppression on diffusion-tensor tractography recently have been evaluated for the corpus callosum (32), but its consequences on subsequent tract-derived quantitative analyses of diffusion parameters and its implications on the fiber tracking of the limbic system have not been examined.

The objectives of this study were 2-fold: (1) to examine the effect of FLAIR for CSF suppression on quantitative diffusion tensor tractography and (2) to report diffusion parameter values along the fornix and cingulum in healthy, young adult volunteers. These results will provide a solid basis to guide future studies of the limbic connections with disease.

Methods

Approval of the research protocol was obtained from the Institutional Health Research Ethics Board of the University of Alberta, and informed consent was obtained from all participants.

Image Acquisition

Nine healthy subjects, with a mean age of 28 ± 5 years (range, 23–36 years) were scanned by using a 1.5T Siemens Sonata scanner (Erlangen, Germany). Both standard and FLAIR DTI sequences used were identical, with the exception of the inversion pulse and the number of sections. Both datasets were acquired by using a dual spin-echo, single shot echo-planar imaging sequence with the following parameters: section thickness, 2 mm; no interslice gap; TR, 10 seconds; TE, 88 ms; field of view, 256 × 256 mm; matrix, 96 × 128 (interpolated to 256 × 256); 6 diffusion directions; b = 1000 s/mm^2; 8 averages. The voxel dimensions at the time of acquisition were 2.67 × 2 × 2 mm, which resulted in voxel dimensions of 1 × 1 × 2 mm after interpolation of the data. The FLAIR DTI sequence used an inversion time (TI) of 2200 ms and acquired 26 sections, whereas the standard (non-FLAIR) DTI acquired 63 sections (acquisition time for both imaging schemes was 9:30 minutes). The section orientation and the center of the sections were identical for both techniques. Because more sections were acquired by using standard DTI, only the 26 sections present in both datasets were used for fiber tracking and further analysis. The calculated SNR on the nondiffusion weighted (b = 0 s/mm^2) images for the standard DTI datasets was, on average, 65 ± 2, whereas that of FLAIR DTI was 47 ± 1.

Fiber Tracking

Tensor processing of the images and fiber tracking were performed on a PC running DTIstudio (Johns Hopkins University, Baltimore, MD), which used the fiber assignment by continuous tracking (FACT) algorithm (13). Tracts were initiated by seeding the entire dataset in those voxels with a FA value > 0.3. The tracts were propagated until they reached a voxel with a FA < 0.3 or if the propagating line deviated by an angle $>70°$.

Tract Selection

Fiber tracking is a 2-step, semiautomatic process in which all tracts are first extracted in the entire dataset by the tracking algorithm as outlined above. Subsequently, individual tracts are selected manually. To dissect a tract virtually, it must be isolated from the original mass of tracts by judicious placement of tract-selection regions drawn (based on a priori anatomical knowledge of tract projections) on the 2D images or maps in any orientation (14, 27, 33). The most common approach is to isolate the tracts by selecting them only if they penetrate one or more such regions. (For example, see Fig 1 in the reports by Catani et al [11] and Wakana et al [27].)

We experimented with several schemes for tract selection by using different locations of tract selection regions. Initially, tracts were selected only if they traversed 2 or more regions drawn at great distance from each other, which caused a great number of tracts to be discarded, because they were shorter in

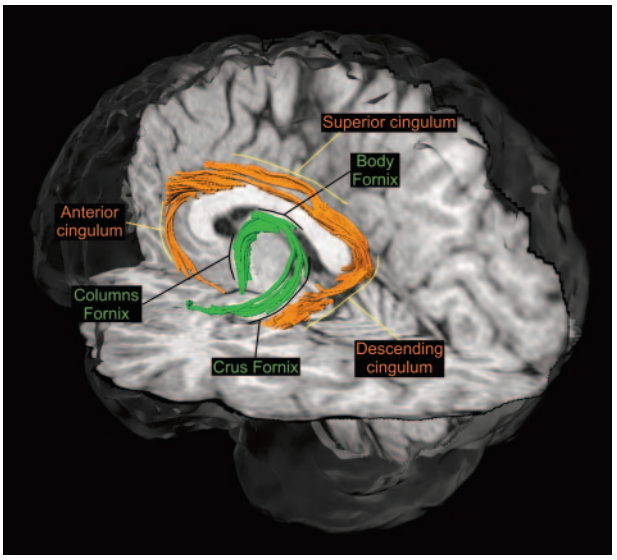

FIG 1. Diffusion tensor tractography of the fornix and cingulum in a healthy individual.

3D fiber tracking of the fornix (*green*) and cingulum (*orange*) overlaid on an anatomical, T1-weighted 3D–magnetization-preparation rapid gradient echo (MPRAGE) volume. The anatomy of these 2 fiber bundles can be thought as 2 nested semicircles. The tracts shown were selected by brute force for display purposes only. The labeled portions of the tracts (indicated by *yellow lines* for the cingulum and *black lines* for the fornix) were analyzed subsequently by using judicious tract selection regions, as shown in Figs 2 and 3.

length, albeit having an anatomically correct orientation. This strict selection scheme, though theoretically appealing, was impractical for the fornix and cingulum. On the other hand, if several regions were drawn closely and tracts were selected if they traversed any of them, there was a tendency to include several erroneous tracts and to overestimate the volume of the bundles. We found that we could use some of the strictness of the first approach, combined with the flexibility of the second, to be able to select medium-length tracts with correct orientation while still restricting their path.

Thus, we selected 3 different portions of each tract separately (Figs 1–3). Tracts were selected if they penetrated a selection region located halfway along the tract, and any of 2 selection regions drawn at the extremes of the portion we wished to study. Tract selection regions and the resulting portions of the tracts that were analyzed are shown in Figs 2 and 3 for the fornix and cingulum, respectively. As can be seen from the figures, the tract selection regions must not precisely outline the tracts, but simply contain them. Tractography and subsequent measurements were performed separately for the right and left fornix and cingulum in each subject.

Diffusion Measurements and Volume Analysis

FA and mean ADC values were queried at each tract's voxel locations by using an in-house program. A single measurement of either FA or mean ADC for each tract portion per subject was calculated by averaging all the voxels present in the tract. The same procedure was followed for both imaging techniques. For volume measurements, the number of voxels containing at least one fiber was counted, and the result was multiplied by 2 mm^3, the interpolated voxel volume.

Tract volume, FA, and mean ADC measurements were restricted to the sections of the tracts between the 2 most extreme tract selection regions, thereby assuring that changes in measurements were not due to longer fibers. The landmarks used for parcellation are shown in Figs 2 and 3 for the fornix and cingulum, respectively.

In light of the sample size, the normality of the data cannot be guaranteed. Therefore, statistically significant differences were assessed by 2-tailed Wilcoxon signed ranks tests for each measurement. Results are reported as significant if they had a P value $\leq .05$.

Results

The Role of FLAIR in Tractography

Overall, tract selection of all the portions of the fornix was easier and more reliable when tracking was performed on FLAIR DTI datasets. In particular, the crus of the fornix could be easily selected in its entirety employing a single tract selection region in 13 of 18 cases when CSF suppression was performed, as opposed to a single case when standard DTI was used (Fig 4). This was due to the fact that the voxels belonging to the crura had FA values (0.15–0.25) below the tracking threshold of 0.3 when no CSF suppression was performed. These particular voxels, alleviated from the deleterious partial volume averaging, increased their FA values to ~0.30–0.40 with the use of FLAIR DTI, which resulted in a continuous fornix from body to crus. The cingulum, on the other hand, did not show this subjective difference in the ease of tract selection in its descending and superior portions. The anterior portion, however, was easier to reconstruct because it typically had a greater number of voxels included when CSF suppression was performed (Table).

As can be seen in the Table, both tracts showed a significant increase in diffusion anisotropy in 2 of their 3 portions when measurements were derived from FLAIR DTI datasets, relative to standard DTI. The most consistent increases of FA occurred at the levels of the crus and body of the fornix, where it occurs concomitantly with a reduction in mean ADC. Although this reduction in mean diffusivity was large (particularly in the body of the fornix), mean ADC values remained high in the fornix when compared with the cingulum, which could be attributed to incomplete CSF suppression at the level of the ventricles due to pulsation artifacts, because cardiac gating was not used in this study (34, 35). Furthermore, there is hardly any reduction in mean ADC at the level of the columns of the fornix, which seems to coincide with the lack of increase in diffusion anisotropy.

The volume of the resulting tracts was significantly increased in all the portions of the fornix and in 2 of 3 portions of the cingulum when DTI was performed with CSF suppression. Such an increase in volume was brought about by the inclusion of more voxels for tractography, because of their increased diffusion anisotropy measurements (above the fiber-tracking FA threshold of 0.3). Furthermore, more voxels with an FA above the tracking threshold translates into more seeding points, which facilitates tract reconstruction.

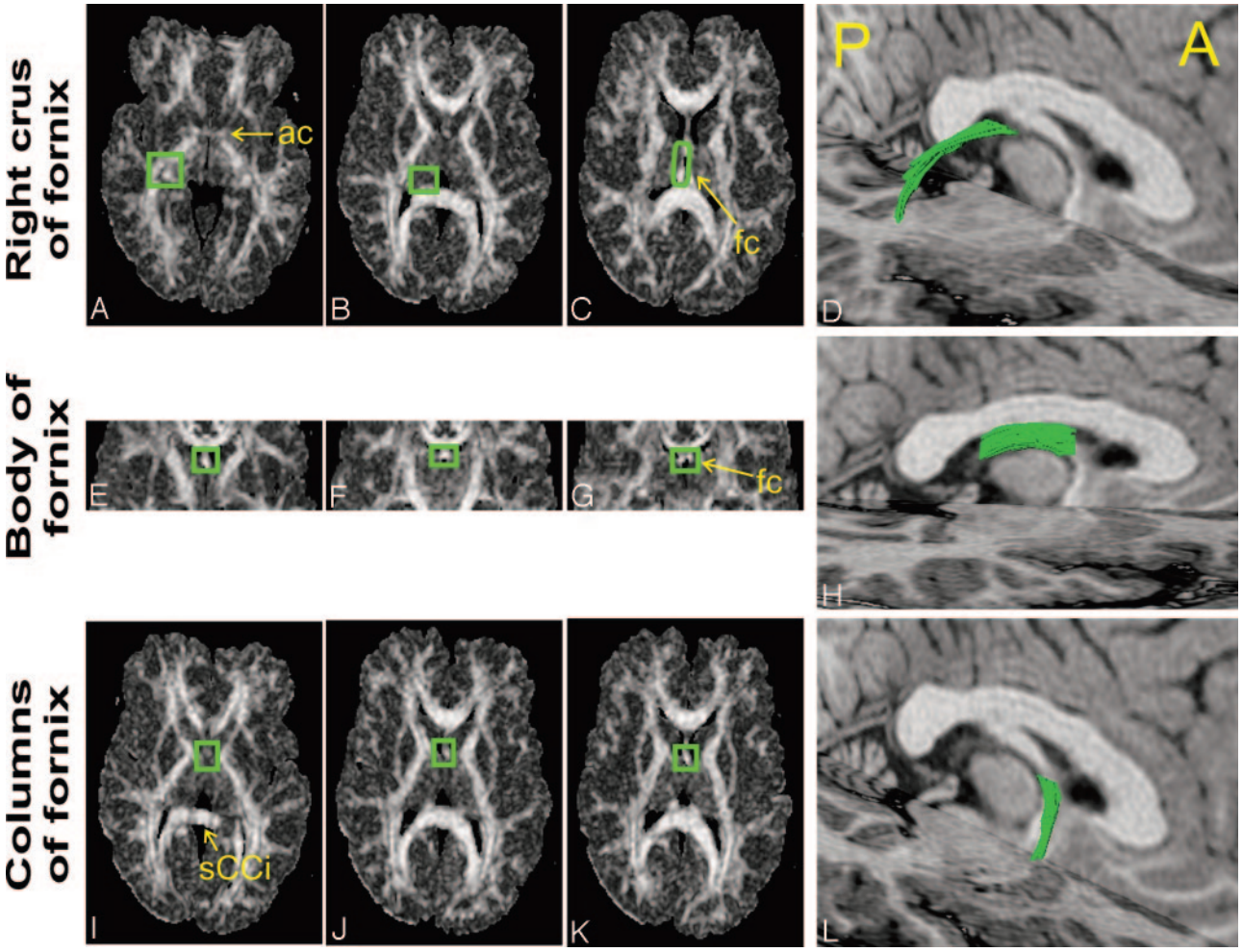

FIG 2. Region of interest placement for selection of individual portions of the fornix.

The fornix was selected in 3 distinct portions, because this enhances the selection accuracy. For each portion, tract-selection regions were manually drawn on either FA or principal diffusivity color maps. To be selected, the tracts had to go through the middle tract-selection region (*B, F,* and *J, green boxes*) and through either one of the extreme regions (*A* or *C; E* or *G; I* or *K,* for the crus, body, and columns, respectively). The FA maps presented are derived from CSF-suppressed DTI. The same procedure was repeated for the standard DTI datasets by using identical tract selection regions. The resulting FLAIR DTI-derived tracts of a healthy subject are presented in 3D views overlaid on anatomic 3D-MPRAGE axial and sagittal sections (*D, H,* and *L*). Subsequent analyses of all segments were performed only between the 2 extreme tract selection regions. A, anterior; P, posterior; ac, anterior commissure; fc, fusion of the crura; sCCi, inferior border of the splenium of the corpus callosum. Panel *E* is 0.5 cm posterior to the vertical AC line. Panel *K* is parallel to the inferior border of the body of the fornix.

Diffusion Characteristics in the Limbic System

We only found asymmetry of diffusion anisotropy in the superior portion of the cingulum (FA right = 0.63 ± 0.02; FA left = 0.66 ± 0.03; $P = .017$), which is consistent with previous studies (16, 17, 19, 20). Because of this, the results presented in the Table show collapsed data per subject (ie, [FA left + FA right]/2). It is clear from the Table that diffusion anisotropy lies within a tight range throughout the limbic system, being highest in the superior portion of the cingulum and the body of the fornix. As with any other brain tissue, mean ADC remains relatively uniform, with the exception of the portions that suffer incomplete CSF suppression in which partial volume averaging persists (ie, body and columns and, to some extent, the crus of the fornix).

Discussion

DTI is rapidly becoming a widely available imaging technique with myriad applications. The possibility of discerning the orientation of white matter bundles and the ability to reconstruct their 3D structure in vivo has opened the door to selective studies of fiber tracts both in healthy and diseased human brain.

DTI can be adversely affected by a number of factors, such as inaccurate sorting of eigenvalues due to low SNR and partial volume averaging (36). Partial volume averaging results when 2 or more different tissue types that are contained within 1 voxel yield an MR imaging signal intensity that is the weighted sum of each tissue's signal intensity. Thus, this artifact is more conspicuous as the voxel size increases (ie, imaging resolution worsens) and when the various tis-

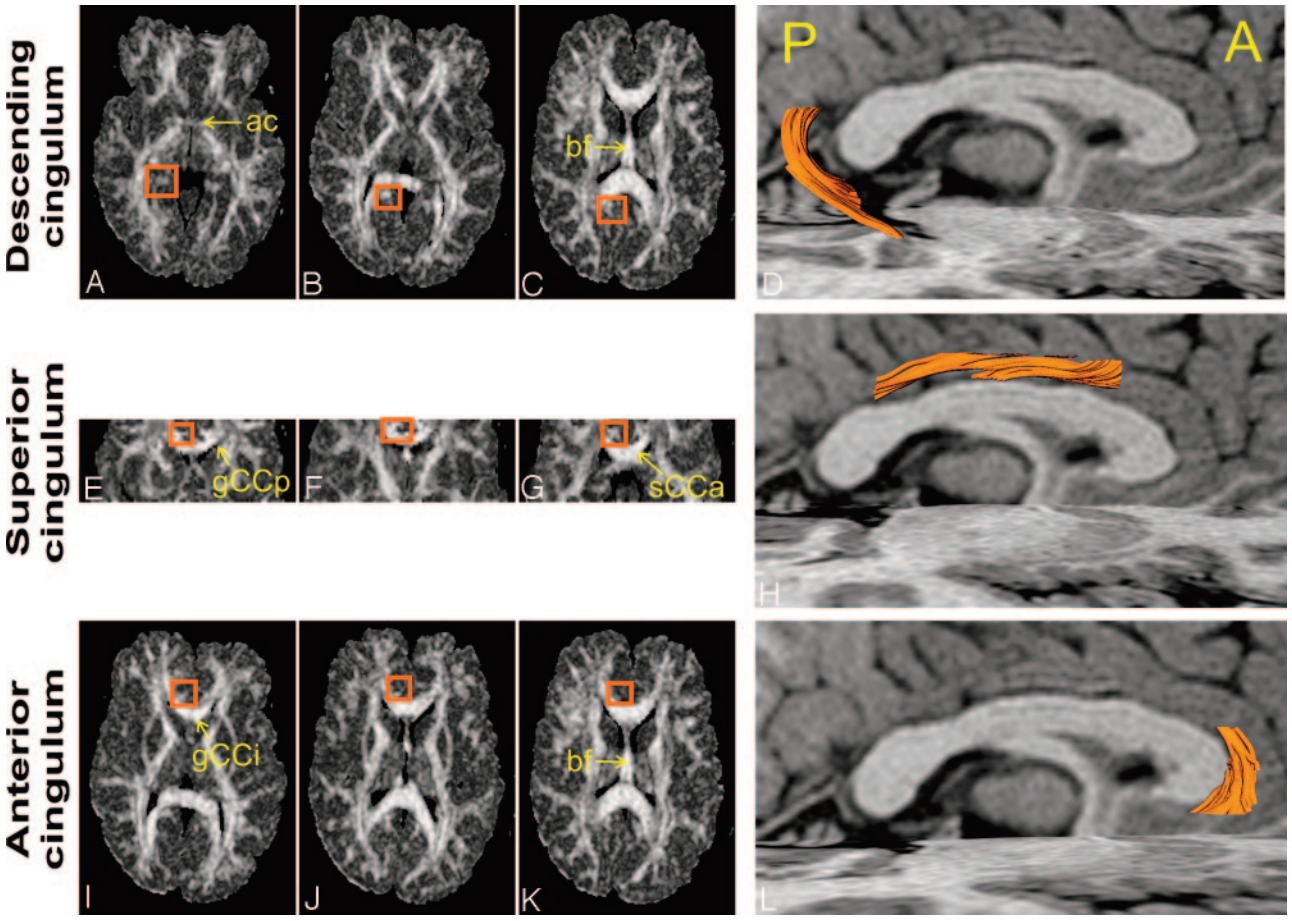

FIG 3. Region of interest placement for selection of individual portions of the cingulum.

Three portions of the cingulum—namely, the descending, superior, and anterior portions—were selected after fiber tracking of the entire volume in both standard and FLAIR DTI datasets. For each portion, tract-selection regions were manually drawn on either FA or principal diffusivity color maps. To be selected, the tracts had to go through the middle tract-selection region (*B, F,* and *J, orange boxes*) and through either one of the extreme regions (*A* or *C; E* or *G; I* or *K,* for the descending, superior, and anterior portions, respectively). The FA maps presented are derived from CSF-suppressed DTI. The same procedure was repeated for the standard DTI datasets by using identical tract selection regions. The resulting FLAIR DTI-derived tracts of a healthy subject are presented in 3D views overlaid on anatomic 3D-MPRAGE axial and sagittal sections (*D, H,* and *L*). Subsequent analyses of all segments were performed only between the 2 extreme tract selection regions. A, anterior; P, posterior; ac, anterior commissure; bf, body of fornix; gCCp, posterior border of the genu of the corpus callosum; sCCa, anterior border of the callosal splenium; gCCi, inferior border of the callosal genu.

sues have vastly different measurable properties. For example, CSF shows fast, isotropic water diffusion as opposed to the slower, highly anisotropic water diffusion seen in white matter tracts. Two approaches can be taken to minimize this artifact. The first is to acquire the images with very small voxels (36), though this can dramatically decrease the SNR. The second approach is to nullify the signal intensity arising from CSF by using an inversion recovery pulse with an inversion time tailored to the T1 of CSF (FLAIR) before the otherwise typical diffusion tensor imaging sequence (29–31). The use of FLAIR has the disadvantages of increasing the scan time due to the longer repetition time required and decreasing the SNR by ~30% (assuming constant repetition time). The increase in scan time per section translated into a smaller brain coverage in FLAIR DTI (26 sections) as opposed to standard DTI (63 sections). On the other hand, diffusion measurements derived from FLAIR DTI represent the underlying tissue more accurately, especially in regions of high CSF contamination, such as near the ventricles and sulci. If precise measurements of diffusion properties of susceptible tissues are sought, the use of FLAIR is recommended and the increased scan time is justified. Although our current imaging sequence could be improved with an increase in the number of diffusion directions and/or averages (37), the repetition time needed to fit the inversion recovery pulse for CSF signal intensity suppression would make the additional acquisition time impractical for a clinical setting.

Diffusion-tensor tractography of the limbic system can, therefore, benefit from FLAIR, because significant portions of the cingulum and fornix are affected by CSF signal intensity contamination. As can be seen in the Table, the tractography algorithm is able to depict thicker tracts when FLAIR is used, particularly in the fornix. Furthermore, the diffusion measurements derived from the FLAIR datasets are more likely to approximate the real tissue properties. The principal eigenvector of an anisotropic diffusion ellipsoid does not change its orientation when an isotropic

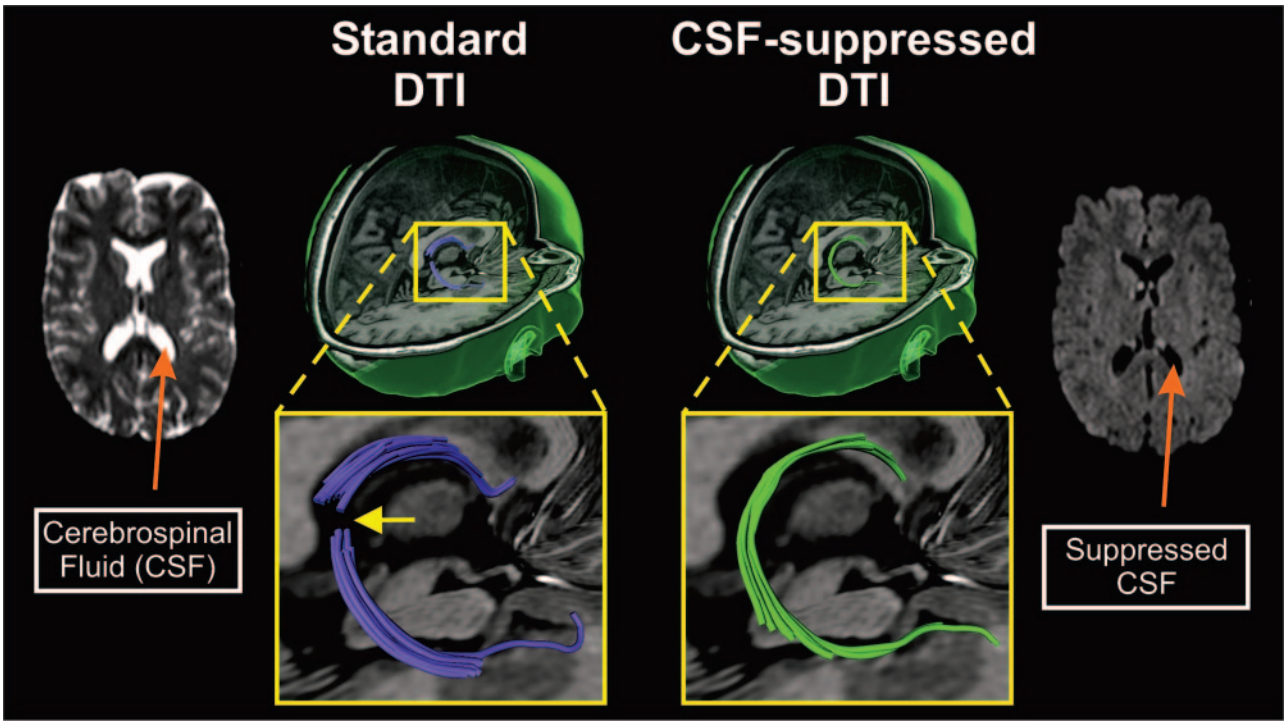

FIG 4. Qualitative assessment of the role of CSF suppression in tractography.

Because of CSF signal intensity contamination, the crus of the fornix is difficult to depict with fiber tracking derived from standard DTI datasets. Tissue voxels belonging to the top portion of the crus of the fornix (*yellow arrow*) suffer partial volume averaging and their diffusion anisotropy drops below the fiber tracking FA threshold (0.3) to values that range from 0.15 to 0.25. When CSF suppression is performed, the same region contains higher anisotropy values (~0.30–0.40) and its voxels are included by the tracking algorithm, which results in a complete depiction of the structure. The axial nondiffusion-weighted images (b = 0 s/mm^2) show the bright CSF signal intensity in standard DTI, which is suppressed with FLAIR DTI. The portions of the fornix are overlaid on T1-weighted, anatomical 3D-MPRAGE axial and sagittal sections.

diffusion tensor is added. Therefore, it is tempting to argue that a simple reduction of the FA threshold would provide accurate tract depictions even in the presence of CSF contamination; however, use of an FA threshold <0.25 for fiber tracking greatly increases the number of erroneous tracts and the variability in tract depictions (25). Furthermore, even if the tract is outlined anatomically correctly, the diffusion parameters, such as mean diffusivity and FA, will be adversely affected by the contaminating CSF signal intensity.

The FACT fiber-tracking algorithm we used (13) reconstructs all the tracts existing in a volume by seeding all the voxels that have an FA greater than a certain threshold (0.3 in our study). With judicious placement of more than one tract selection region, it is not necessary to precisely outline the bundle of interest, but merely to contain it within a well-defined area. Although this reduces the user dependence on tract selection, it is still necessary to follow the same general guidelines for all subjects in a study.

We saw important improvements both in the overall appearance of the tracts and the diffusion measurements derived from them when CSF suppression was performed. This was particularly important in the anterior portion of the cingulum and the crus and body of the fornix. The anterior portion of the cingulum travels very close to the CSF present in the interhemispheric fissure, which could be responsible for the reduced FA and number of voxels included in the tract derived from standard DTI. The 3 portions of the fornix studied are bathed by CSF, which accounts for the significant differences of FA and mean ADC seen in the crus and body when FLAIR is used. These changes in diffusion anisotropy were in part responsible for the improved reconstruction of the tracts (Fig 4). It is interesting to note that the columns of the fornix did not show a significant increase in FA or a decrease in mean ADC as would be expected.

Previous studies have reported mean ADC values to lie in the vicinity of 0.7×10^{-3} mm^2/s throughout the white matter (31, 38). Overall, mean ADC values in all portions of the fornix were higher than those expected. This could be due to incomplete CSF suppression by the inversion pulse, which occurs when noninverted spins in CSF enter the imaging section as a result of pulsation (34, 35). Incomplete CSF suppression could also be responsible for the absence of changes in the columns of the fornix when FLAIR was used. Cardiac gating has been shown to minimize pulsation artifacts (39, 40), but, because of its nature, its combination with an inversion-recovery pulse for CSF suppression is not straightforward. Nevertheless, alternative CSF-suppression techniques that are insensitive to pulsation exist (41, 42), but their use has not yet become widespread and were not evaluated in this study.

Previous studies have evaluated FA in the superior

Diffusion parameters and volume of limbic connections

	Cingulum			Fornix		
	Descending	Superior	Anterior	Crus	Body	Columns
FA						
Standard	0.48 ± 0.02	0.66 ± 0.02	0.44 ± 0.02	0.49 ± 0.02	0.54 ± 0.05	0.52 ± 0.02
FLAIR	0.50 ± 0.02	0.65 ± 0.03	0.48 ± 0.03	0.53 ± 0.02	0.61 ± 0.03	0.54 ± 0.03
Difference	0.02 ± 0.01	−0.01 ± 0.01	0.05 ± 0.03	0.03 ± 0.02	0.07 ± 0.05	0.01 ± 0.04
P	.011	.04	.027	.011	.015	.29
Mean ADC ($\times 10^{-3}$ mm^2/s)						
Standard	0.75 ± 0.03	0.71 ± 0.02	0.72 ± 0.03	0.96 ± 0.1	1.45 ± 0.1	0.99 ± 0.07
FLAIR	0.75 ± 0.02	0.72 ± 0.01	0.73 ± 0.03	0.89 ± 0.04	1.0 ± 0.04	0.95 ± 0.06
Difference	0 ± 0.02	0.01 ± 0.01	0.01 ± 0.01	−0.06 ± 0.08	−0.44 ± 0.13	−0.04 ± 0.08
P	1.0	.14	.16	.05	.008	.16
Volume (mm^3)						
Standard	504 ± 136	1196 ± 504	168 ± 30	244 ± 136	572 ± 96	174 ± 44
FLAIR	600 ± 196	1508 ± 492	260 ± 72	540 ± 130	724 ± 126	292 ± 110
Difference	110 ± 120	312 ± 391	120 ± 43	196 ± 87	150 ± 138	118 ± 81
P	.123	.036	.018	.008	.015	.011

Note.—FA indicates fractional anisotropy; ADC, apparent diffusion coefficient; FLAIR, fluid-attenuated inversion recovery.

FA, mean ADC, and volume (mean ± SD) are presented for 3 portions of the fornix and cingulum depicted with tractography derived from diffusion tensor imaging datasets with and without CSF suppression (FLAIR and Standard, respectively). Except for the superior portion of the cingulum, all structures showed no interhemispheric asymmetry and are therefore presented as collapsed data; that is (left + right)/2. FLAIR diffusion tensor imaging resulted in significant increases of fractional anisotropy in the descending and anterior portions of the cingulum, crus, and body of the fornix, as well as decreases of mean ADC in the crus and body of the fornix. A significant increase in tract volume with CSF suppression was also observed in 5 of 6 tract portions.

and anterior portions of the cingulum in healthy controls, though the nomenclature used for the different portions of these tracts varies among reports. Sun et al (18) performed region of interest analysis of the anterior section of the cingulum (in the boundaries between the superior and anterior portions, as defined this study) and reported an FA of 0.64, which is similar to the values we found in the superior portion of the cingulum. Wang et al (20) found an average FA of 0.51 for the left and 0.44 for the right hemisphere by using multisection regions of interest located in approximately the same region as that described by Sun et al. They also analyzed the region between the superior and descending portions of the cingulum and reported FAs of 0.39 and 0.42 for the left and right hemispheres, respectively. These 2 areas were not analyzed in our present study. Kubicki et al (17) found average FA values of 0.50 and 0.47, respectively, for the left and right superior portions of the cingulum of healthy controls in a multisection, segmentation-based analysis, which is lower than our FA findings of 0.66 and 0.63 (left and right, respectively) by using FLAIR DTI. By using tract-based analysis, Gong et al (16) radially divided the cingulum in 2 sections: one that contains the anterior portion and half of the superior portion (as described in our study) and another that comprises the posterior half of the superior portion of the cingulum. They found the posterior half to have higher FA values than the anterior half, though they were in general lower (~0.35 and ~0.45 for the anterior and posterior sections) than those we report. It is important to notice that previous studies have not used CSF-suppressed DTI and that they employ a different analysis method than the one described here. We recently reported diffusion measurements for the descending portion of the cingulum and the crus of the fornix in healthy individuals and in patients with mesial temporal lobe sclerosis (21), but the remaining portions of these tracts were not evaluated in our prior study.

At the current resolution that DTI can achieve in a clinical setting, it is not possible to perform tractography of other limbic connections, such as the mammillo-thalamic tract or the anterior thalamic radiations. Our findings, however, suggest that tractography-based DTI analysis of the fornix and cingulum can provide reproducible findings and that this information can be used to indirectly study the axonal integrity of white matter tracts within the limbic system in a variety of brain disorders.

Conclusions

As expected from previous studies using 2D DTI analysis, diffusion-tensor tractography benefits from CSF suppression, in both the ease for fiber tracking and tract selection and the diffusion measurements derived from the delineated tracts. This is particularly true if the tract of interest is near CSF spaces, such as the fiber bundles of the limbic system, which justifies the increased scan time and acceptable reduction in SNR. A similar benefit could be anticipated in any other tract near CSF spaces, such as the corpus callosum.

When a strict tract-selection method is used, the fornix and cingulum can be reliably depicted by using diffusion tensor tractography. Because there is small intersubject variability in diffusion measurements in these 2 important and very interesting limbic connections, this technique is applicable for clinical research

in a variety of patient populations. We recommend the use of CSF suppression when performing tractography of limbic connections.

Acknowledgments

MR imaging infrastructure was from the Canada Foundation in Innovation, AB Science and Research Authority, AB Heritage Foundation for Medical Research, and the University Hospital Foundation. Fiber tracking software kindly provided by Drs. Hangyi Jiang and Susumu Mori (National Institutes of Health grant P41 RR15241–01).

References

1. Mark LP, Daniels DL, Naidich TP, Borne JA. **Limbic system anatomy: an overview.** *AJNR Am J Neuroradiol* 1993;14:349–352
2. Papez J. **A proposed mechanism of emotion.** *Arch Neurol Pathol* 1937;38:725–743
3. Ng SE, Lau TN, Hui FK, et al. **MRI of the fornix and mamillary body in temporal lobe epilepsy.** *Neuroradiology* 1997;39:551–555
4. Kuzniecky R, Bilir E, Gilliam F, et al. **Quantitative MRI in temporal lobe epilepsy: evidence for fornix atrophy.** *Neurology* 1999; 53:496–501
5. Oikawa H, Sasaki M, Tamakawa Y, Kamei A. **The circuit of Papez in mesial temporal sclerosis: MRI.** *Neuroradiology* 2001;43:205–210
6. Kodama F, Ogawa T, Sugihara S, et al. **Transneuronal degeneration in patients with temporal lobe epilepsy: evaluation by MR imaging.** *Eur Radiol* 2003;13:2180–2185
7. Bernasconi N, Duchesne S, Janke A, et al. **Whole-brain voxel-based statistical analysis of gray matter and white matter in temporal lobe epilepsy.** *Neuroimage* 2004;23:717–723
8. Smith CD, Malcein M, Meurer K, et al. **MRI temporal lobe volume measures and neuropsychologic function in Alzheimer's disease.** *J Neuroimaging* 1999;9:2–9
9. Callen DJ, Black SE, Gao F, et al. **Beyond the hippocampus: MRI volumetry confirms widespread limbic atrophy in AD.** *Neurology* 2001;57:1669–1674
10. Zahajszky J, Dickey CC, McCarley RW, et al. **A quantitative MR measure of the fornix in schizophrenia.** *Schizophr Res* 2001; 47:87–97
11. Catani M, Howard RJ, Pajevic S, Jones DK. **Virtual in vivo interactive dissection of white matter fasciculi in the human brain.** *Neuroimage* 2002;17:77–94
12. Jones DK, Simmons A, Williams SC, Horsfield MA. **Non-invasive assessment of axonal fiber connectivity in the human brain via diffusion tensor MRI.** *Magn Reson Med* 1999;42:37–41
13. Mori S, Crain BJ, Chacko VP, van Zijl PC. **Three-dimensional tracking of axonal projections in the brain by magnetic resonance imaging.** *Ann Neurol* 1999;45:265–269
14. Conturo TE, Lori NF, Cull TS, et al. **Tracking neuronal fiber pathways in the living human brain.** *Proc Natl Acad Sci U S A* 1999;96:10422–10427
15. Mori S, van Zijl PC. **Fiber tracking: principles and strategies: a technical review.** *NMR Biomed* 2002;15:468–480
16. Gong G, Jiang T, Zhu C, et al. **Asymmetry analysis of cingulum based on scale-invariant parameterization by diffusion tensor imaging.** *Hum Brain Mapp* 2005;24:92–98
17. Kubicki M, Westin CF, Nestor PG, et al. **Cingulate fasciculus integrity disruption in schizophrenia: a magnetic resonance diffusion tensor imaging study.** *Biol Psychiatry* 2003;54:1171–1180
18. Sun Z, Wang F, Cui L, et al. **Abnormal anterior cingulum in patients with schizophrenia: a diffusion tensor imaging study.** *Neuroreport* 2003;14:1833–1836
19. Park H-J, Westin C-F, Kubicki M, et al. **White matter hemisphere asymmetries in healthy subjects and in schizophrenia: a diffusion tensor MRI study.** *Neuroimage* 2004;23:213–223
20. Wang F, Sun Z, Cui L, et al. **Anterior cingulum abnormalities in male patients with schizophrenia determined through diffusion tensor imaging.** *Am J Psychiatry* 2004;161:573–575
21. Concha L, Beaulieu C, Gross DW. **Bilateral limbic diffusion abnormalities in unilateral temporal lobe epilepsy.** *Ann Neurol* 2005;57:188–196
22. Friston KJ, Holmes AP, Worsley KJ, et al. **Statistical parametric maps in functional imaging: a general linear approach.** *Hum Brain Mapp* 1995;2:189–210
23. Ashburner J, Friston KJ. **Voxel-based morphometry: the methods.** *Neuroimage* 2000;11:805–821
24. Xue R, van Zijl PC, Crain BJ, et al. **In vivo three-dimensional reconstruction of rat brain axonal projections by diffusion tensor imaging.** *Magn Reson Med* 1999;42:1123–1127
25. Stieltjes B, Kaufmann WE, van Zijl PC, et al. **Diffusion tensor imaging and axonal tracking in the human brainstem.** *Neuroimage* 2001;14:723–735
26. Mori S, Kaufmann WE, Davatzikos C, et al. **Imaging cortical association tracts in the human brain using diffusion-tensor-based axonal tracking.** *Magn Reson Med* 2002;47:215–223
27. Wakana S, Jiang H, Nagae-Poetscher LM, et al. **Fiber tract-based atlas of human white matter anatomy.** *Radiology* 2004;230:77–87
28. Hajnal JV, Bryant DJ, Kasuboski L, et al. **Use of fluid attenuated inversion recovery (FLAIR) pulse sequences in MRI of the brain.** *J Comput Assist Tomogr* 1992;16:841–844
29. Papadakis NG, Martin KM, Mustafa MH, et al. **Study of the effect of CSF suppression on white matter diffusion anisotropy mapping of healthy human brain.** *Magn Reson Med* 2002;48:394–398
30. Ma X, Kadah YM, LaCorte SM, Hu X. **Enhancing measured diffusion anisotropy in gray matter by eliminating CSF contamination with FLAIR.** *Magn Reson Med* 2004;51:423–427
31. Bhagat YA, Beaulieu C. **Diffusion anisotropy in subcortical white matter and cortical gray matter: changes with aging and the role of CSF-suppression.** *J Magn Reson Imaging* 2004;20:216–227
32. Chou MC, Lin YR, Huang TY, et al. **FLAIR diffusion-tensor MR tractography: comparison of fiber tracking with conventional imaging.** *AJNR Am J Neuroradiol* 2005;26:591–597
33. Melhem ER, Mori S, Mukundan G, et al. **Diffusion tensor MR imaging of the brain and white matter tractography.** *AJR Am J Roentgenol* 2002;178:3–16
34. Adams JG, Melhem ER. **Clinical usefulness of T2-weighted fluid-attenuated inversion recovery MR imaging of the CNS.** *AJR Am J Roentgenol* 1999;172:529–536
35. Bakshi R, Caruthers SD, Janardhan V, Wasay M. **Intraventricular CSF pulsation artifact on fast fluid-attenuated inversion-recovery MR images: analysis of 100 consecutive normal studies.** *AJNR Am J Neuroradiol* 2000;21:503–508
36. Basser PJ, Pierpaoli C. **Microstructural and physiological features of tissues elucidated by quantitative-diffusion-tensor MRI.** *J Magn Reson B* 1996;111:209–219
37. Jones DK, Williams SC, Gasston D, et al. **Isotropic resolution diffusion tensor imaging with whole brain acquisition in a clinically acceptable time.** *Hum Brain Mapp* 2002;15:216–230
38. Pierpaoli C, Jezzard P, Basser PJ, et al. **Diffusion tensor MR imaging of the human brain.** *Radiology* 1996;201:637–648
39. Brockstedt S, Borg M, Geijer B, et al. **Triggering in quantitative diffusion imaging with single-shot EPI.** *Acta Radiol* 1999;40: 263–269
40. Skare S, Andersson JL. **On the effects of gating in diffusion imaging of the brain using single shot EPI.** *Magn Reson Imaging* 2001; 19:1125–1128
41. Herlihy AH, Hajnal JV, Curati WL, et al. **Reduction of CSF and blood flow artifacts on FLAIR images of the brain with k-space reordered by inversion time at each slice position (KRISP).** *AJNR Am J Neuroradiol* 2001;22:896–904
42. Herlihy AH, Oatridge A, Curati WL, et al. **FLAIR imaging using nonselective inversion pulses combined with slice excitation order cycling and k-space reordering to reduce flow artifacts.** *Magn Reson Med* 2001;46:354–364